A Multimodal Imaging Analysis of Subcortical Gray Matter in Fragile X Premutation Carriers

Jun Yi Wang, PhD,[1,2] Randi J. Hagerman, MD,[3,4] and Susan M. Rivera, PhD[1,3,5]*

[1]Center for Mind and Brain, University of California–Davis, Davis, California, USA
[2]Department of Psychiatry and Behavioral Sciences, University of California–Davis, School of Medicine, Sacramento, California, USA
[3]Medical Investigation of Neurodevelopmental Disorders (MIND) Institute, University of California–Davis Medical Center, Sacramento, California, USA
[4]Department of Pediatrics, University of California–Davis, School of Medicine, Sacramento, California, USA
[5]Department of Psychology, University of California–Davis, Davis, California, USA

ABSTRACT: Approximately 40% of males with the fragile X premutation develop fragile X–associated tremor/ataxia syndrome after age 50. Although the thalamus and basal ganglia play a crucial role in movement disorders, their involvement in fragile X premutation carriers has not been systematically investigated. The current study characterized structural abnormalities associated with fragile X premutation carriers (with and without fragile X–associated tremor/ataxia syndrome) in the thalamus, caudate nucleus, putamen, and globus pallidus using T1-weighted and diffusion tensor imaging. Male premutation carriers with fragile X–associated tremor/ataxia syndrome showed significant volume atrophy and diffusion-weighted signal loss in all 4 structures compared with the control group. They also exhibited volume atrophy and diffusion-weighted signal loss in the thalamus and striatum compared with the premutation carriers without fragile X–associated tremor/ataxia syndrome. Importantly, many of the meas- urements exhibited robust correlations with symptom severity, with volume and diffusion-weighted imaging measurements displaying negative correlations and fractional anisotropy measurements displaying positive correlations. The current study demonstrated involve- ment of all 4 subcortical gray matter structures in fragile X–associated tremor/ataxia syndrome, with significant volume atrophy, and possible iron deposition indicated by the diffusion-weighted signal loss. The significant correlation between the subcortical measurements and symptom severity suggests the benefits of tracking structural changes in subcortical gray matter in future longitudinal studies for early detection and disease monitoring. © 2013 *Movement* Disorder Society

Key Words: neurodegeneration; iron dysregulation; genetic disorder; diffusion tensor imaging; diffusion-weighted imaging

The fragile X mental retardation 1 (*FMR1*) gene has a polymorphic CGG repeat in its 5′ untranslated region that normally ranges from 5 to 44 triplets.[1]

Premutation alleles with expansions of the CGG repeat to 55–200 triplets are relatively common in the general population, representing a prevalence rate of 1:110–250 in females and 1:250–810 in males.[2–4] Among males with the premutation alleles of the *FMR1* gene, approximately 40% develop a late-onset neurodegenerative disorder, fragile X–associated tremor/ataxia syndrome (FXTAS), after 50 years of age.[5,6] The principal clinical features associated with FXTAS are progressive intention tremor and gait ataxia, although in a subset of the patients other fea- tures are also present including parkinsonism, periph- eral neuropathy, autonomic dysfunction, executive function deficits, and psychiatric disorders.[7–11] Bio- chemical studies of FXTAS have revealed intranuclear inclusions in the central and peripheral nervous sys- tems, white matter damage throughout the cerebrum

TABLE 1. Characteristics of 61 research participants: mean (SD) [range]

Characteristics	HC (n = 14)	NFPC (n = 11)	FXTAS (n = 36)
Age (y)	61.6 (7.7) [52–81]	60.1 (10.6) [47–76]	65.8 (7.1) [50–79]
FMR1 CGG repeat size	28.2 (6.0) [19–42]	80.5 (17.2) [59–113]	96.5 (20.9) [62–154]
FMR1 mRNA level	1.5 (0.2) [1.0–1.8]	2.5 (0.8) [1.4–4.1]	3.1 (0.8) [1.6–5.6]

NFPC, non-FXTAS premutation carriers; HC, healthy controls.

and cerebellum,[12–14] and disturbed zinc and iron metabolism that leads to iron accumulation in the cells and mitochondrial dysfunction.[15–17]

Disturbed iron homeostasis commonly affects motor functioning in various neurodegenerative disorders[18] because of the high iron concentration and physiology of the extrapyramidal system.[19–21] Given the evidence of deregulated iron metabolism[16] and motor deficits as the primary clinical symptoms,[5,10] it is highly likely that FXTAS involves the extrapyramidal system. Indeed, structural abnormalities in the extrapyramidal structures including the cerebellar peduncles and pontine areas in premutation carriers with and without FXTAS have been reported.[22,23] However, the involvement of the thalamus and basal ganglia in premutation carriers has not previously been systematically examined.

Structural damage in the subcortical gray matter may manifest as changes in volume, tissue microstructure, or iron concentration, all of which can be quantified using different MRI techniques. High-resolution T1-weighted imaging is commonly used for detecting macroscopic changes in volume. Diffusion tensor imaging (DTI)[24,25] has been applied broadly for characterizing tissue microstructure, commonly in white matter but also recently in subcortical gray matter,[26,27] where organized white matter tracts pass through and produce anisotropic water diffusion.[28–30] Diffusion-weighted imaging (DWI) traditionally has been used for detecting cytotoxic edema in strokes.[31,32] However, a recent report[26] extended its utility to quantify iron concentration in subcortical gray matter, supported by the strong correlation between DWI hypointense signals and high iron concentration in the thalamus and putamen in healthy adults.

The current investigation aimed to characterize potential structural damage associated with the fragile X premutation in subcortical gray matter. We used T1-weighted and DTI scans and took a multimodal-imaging analysis approach to measure volume, structural integrity, and iron deposition. Based on existing evidence, we predicted volume atrophy, structural integrity impairment, and DWI-signal loss in subcortical gray matter in patients with FXTAS as well as in premutation carriers without FXTAS, although to a lesser extent.

Patients and Methods

Research Participants

We studied 61 adult men (age, 47–81 years) recruited for an ongoing study of fragile X premutation carriers: 14 healthy controls, 11 premutation carriers without FXTAS, and 36 premutation carriers diagnosed with FXTAS (Table 1). Only age significantly differed in the 2 premutation groups (t_{45} = 2.05, P = .046). The controls and 26 of the premutation carriers were studied in a recent investigation of abnormal age-related changes in structural connectivity in fragile X premutation.[23] All participants signed informed consent according to the study protocols approved by the institutional review boards at the University of California Davis Medical Center.

Premutation alleles were identified using *FMR1* DNA testing (Table 1).[33,34] FXTAS severity was assessed using FXTAS stage.[35] Of the 11 carriers without FXTAS, 7 were given a stage of 0 (no signs of FXTAS), and 4 were given a stage of 1 (subtle or questionable tremor/balance problems with no interference in daily living). Structured clinical interviews for DSM-IV did not find a significantly higher rate of psychiatric problems in stage 1 carriers (2 of 4 with lifetime mood disorder) compared with stage 0 premutation carriers (2 of 7 with lifetime mood disorder and/or current anxiety disorder)—odds ratio, 2.5; 2-tailed P = .47. Of the 36 carriers with FXTAS, 10 were at FXTAS stage 2 (minor tremor/balance problems with minor interference in daily living), 11 at stage 3 (moderate tremor/balance problems with significant interference in daily living), 12 at stage 4 (severe tremor/balance problems requiring a cane or walker), and 3 at stage 5 (use of a wheelchair on a daily basis).

MRI Acquisition Protocol

Neuroimaging was performed on a Trio 3T MRI scanner with an 8-channel head coil (Siemens Medical Solutions, Erlangen, Germany). All images were acquired between 2007 and 2009 before a major scanner upgrade, which caused DTI scans acquired before and after the upgrade to be incomparable. High-resolution T1-weighted MPRAGE scans were acquired in 208 sagittal slices of 0.95-mm thickness (no gap) with a 243-mm FOV, a 256 × 256 matrix interpolated to

512 × 512, a 2500-ms TR, a 4.33-ms TE, and a 7° flip angle. DTI scans with 30 gradient directions were obtained using a single-shot diffusion-weighted EPI sequence in 72 axial sections of 1.9-mm thickness (no gap) with a 243-mm FOV, a 128 × 128 matrix, a 11,900-ms TR, and a 92-ms TE. The diffusion sensitizing gradients were applied at a b value of 700 s/mm^2. Five additional images with minimum diffusion weighting were also obtained.

Image Segmentation

We performed automatic segmentation on the T1-weighted scans using FMRIB's Integrated Registration and Segmentation Tool,[36] distributed with the FMRIB Software Library (FSL; http://www.fmrib.ox.ac.uk/fsl/; University of Oxford, Oxford, England). FIRST takes the Bayesian approach to determine structural boundaries based on shape (manually predefined) and image intensity. We selected the thalamus, caudate nucleus, putamen, and globus pallidus for the analysis. The segmentations were checked and manually corrected for errors using FSLView from FSL.[37] Then masks were generated from the resulting segmentation and eroded 1 voxel for the putamen and pallidus, 2 voxels for the caudate, and 3 voxels for the thalamus using the FSL function *fslmaths*. The amount of erosion was determined after superimposing the masks on coregistered mean diffusivity (MD) maps generated from DTI (see below) to avoid contamination from the cerebrospinal fluid (see Fig. 1).

Image Registration

DTI images were first corrected for motion and eddy current using the eddy_correct function from FSL. DTI Studio (http://cmrm.med.jhmi.edu/; Johns Hopkins Medical Institute, Baltimore, MD) was then used for calculating tensor and generating mean $b0$ images, DWI images (ie, the average of all images with diffusion weighting), and fractional anisotropy (FA) and MD maps. FreeSurfer (http://surfer.nmr.mgh.harvard.edu; Athinoula A. Martinos Center for Biomedical Imaging, Charlestown, MA) was used for coregistering MD maps with T1 (in FreeSurfer space) and then transforming the MD maps to each subject's native space. The coregistration was inspected and manually adjusted to maximize the match of the lateral ventricles between the T1 and MD maps. The resulting transforming matrices were then applied to the FA maps and $b0$ and DWI images. Finally, the FSL tool *fslstats* was used to calculate the volume and average values of FA, MD, and DWI for each mask.

Statistical Analyses

For group comparisons, multiple linear regression was conducted using age and group as independent variables and individual brain measurements (ie, the volume, FA, MD, and DWI of 8 subcortical gray matter areas) as dependent variables. Total cranial volume (TCV) calculated using Sienax from FSL[38] was used as an additional covariate for volume. Benjamini-Hochberg's false discovery rate (FDR),[39] at 5%, was used to correct for multiple comparisons for each type of measurements. O'Brien's test for homogeneity of variance[40] (http://www.mathworks.com/matlabcentral/file exchange/3510-homvar/content/OBrientest.m) was conducted to test for differences in variance across diagnostic groups. Assumptions of the regression models were checked and verified in the data. In addition, ordinal regression using a proportional odds model was performed to predict FXTAS stage from brain measurements, using age as a covariate for FA, MD, and DWI and both age and TCV for volume. The FXTAS variable was recoded so that the model predicted the odds of being in higher FXTAS stages. Assumptions of the proportional odds model were checked and were met except where noted. For the O'Brien's tests and ordinal regression, FDR was applied to all tests that were performed, and the threshold was set at 5%. We report uncorrected P values and specifically indicate significant results according to the FDR procedure. The statistical tests were carried out using Matlab scripts (The Mathworks Inc. Natick, MA) except for ordinal regression, which was conducted using SPSS (IBM Corp. White Plains, NY).

Results
Group Comparisons

Figure 2 displays the group means and SDs of the subcortical structures. As some of the FA and MD measurements showed high intersubject variability in the premutation groups, O'Brien's test for homogeneity of variance[40] was performed to detect potential differences in variances. None of the FA and MD measurements showed significant differences in variances at 5% FDR, although the MD of the left thalamus and left globus pallidus exhibited differences in variances at raw $P < .05$ ($F_{2,58} = 3.6$ and 4.5, $P = .03$ and $.02$, respectively).

For the comparisons of group means, although none of the areas displayed significantly reduced volume in the non-FXTAS group, 6 of the 8 subcortical areas showed significant atrophy in the FXTAS group compared with the control group. These were the bilateral thalamus and putamen, left caudate, and right pallidus. In addition, the FXTAS group exhibited significant DWI hypointensity in the bilateral thalamus, caudate, putamen, and right pallidus compared with the controls. In the comparisons between FXTAS and non-FXTAS groups, the FXTAS group showed volume atrophy in the bilateral thalamus and putamen and DWI
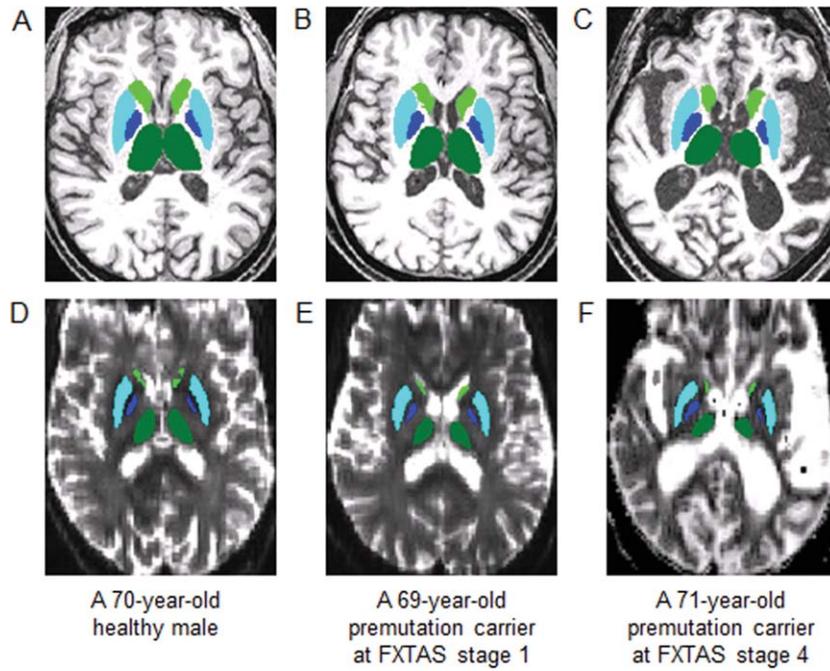
FIG. 1. Segmentation of subcortical gray matter. **A–C:** T1-weighted images. **D–F:** MD maps. Green, thalamus; light green, caudate nucleus; light blue, putamen; blue, globus pallidus.

signal loss in the bilateral putamen, right thalamus, and left caudate (Table 2). In contrast, no differences between any of the groups in FA or MD were detected.

Correlation with FXTAS Stage

We further tested the functional significance of the changes in the subcortical gray matter by conducting ordinal regression analyses to predict FXTAS stage, combining the FXTAS and non-FXTAS groups (n = 47). For the volume measurements, the bilateral thalamus and putamen and left caudate showed significant negative correlations with FXTAS stage after adjusting for age and TCV. In addition, the FA of the bilateral caudate showed significant positive correlation with FXTAS, and DWI of the left caudate and right putamen showed negative correlation after adjusting for age (Table 3). To verify whether the tests
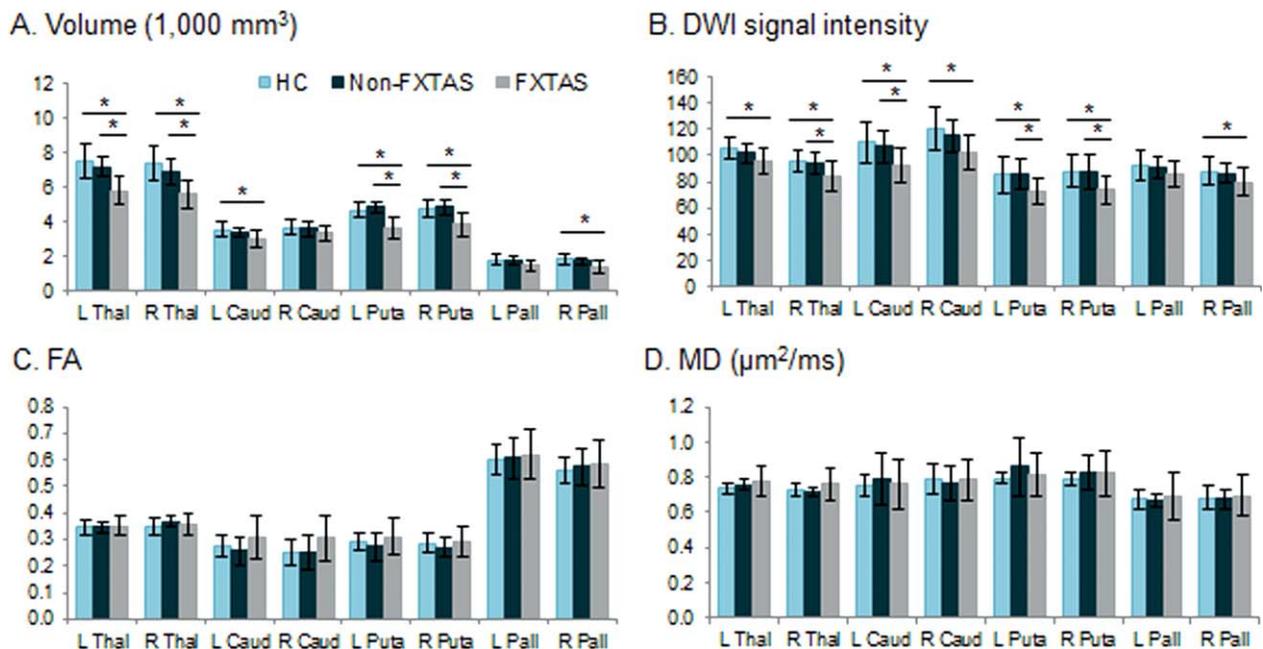
FIG. 2. Group mean and SD of subcortical gray matter structures. *Significant group mean difference at 5% FDR, $P \leq .015$ for volume and $P \leq .021$ for DWI.

TABLE 2. Multiple linear regression analysis of the group effect using TCV (for volume only) and age as covariates

Measurements	NFPC vs HC		FXTAS vs HC		FXTAS vs NFPC	
	t	P	t	P	t	P
Volume						
Thalamus (left)	−1.43	.16	−5.96	**<.001**	3.86	**<.001**
Thalamus (right)	−1.89	.06	−5.80	**<.001**	3.21	**.002**
Caudate (left)	−1.39	.17	−2.71	**.009**	0.94	.351
Caudate (right)	−0.59	.56	−1.04	.301	0.30	.764
Putamen (left)	0.78	.44	−4.87	**<.001**	5.30	**<.001**
Putamen (right)	0.13	.90	−3.78	**<.001**	3.59	**.001**
Pallidus (left)	−0.99	.32	−2.04	.046	0.77	.446
Pallidus (right)	−1.64	.11	−3.58	**.001**	1.47	.148
DWI						
Thalamus (left)	−0.87	.39	−3.18	**.002**	1.89	.064
Thalamus (right)	−0.47	.64	−3.49	**.001**	2.62	**.011**
Caudate (left)	−0.76	.45	−3.77	**<.001**	2.55	**.013**
Caudate (right)	−0.95	.35	−3.71	**<.001**	2.28	.027
Putamen (left)	−0.05	.96	*−2.95*	**.005**	*2.61*	**.012**
Putamen (right)	−0.24	.81	−3.62	**.001**	2.99	**.004**
Pallidus (left)	−0.13	.90	−2.18	.033	1.82	.073
Pallidus (right)	−0.34	.73	−2.54	**.014**	1.91	.062

In boldface, significant at 5% FDR, $P \leq .015$ for volume and .021 for DWI. NFPC, non-FXTAS premutation carriers; HC, healthy controls.

met the proportional odds assumption (ie, the odds ratio for the association between the independent variable and dichotomized FXTAS stage is the same regardless of what cut point is used for dichotomizing FXTAS stage), we checked the results of the likelihood ratio test. At an α level of .05, 2 measurements, right thalamic volume and left caudate DWI, did not pass the test. To exclude the possibility that the relationships between the brain measurements and FXTAS stage were mostly driven by the differences between FXTAS and non-FXTAS patients, we further performed ordinal regression including only the FXTAS patients (n = 36) for these 2 measurements. Although the correlation between right thalamic volume and

FXTAS stage remained significant (odds ratio, 1.14; 95% CI, 1.03–1.25; $P = .008$), left caudate DWI no longer correlated with FXTAS stage (odds ratio, 1.02; 95% CI, 0.97–1.07; $P = .46$).

Discussion

We applied multimodal imaging analysis to characterize the extent and type of structural damage in the subcortical gray matter in male premutation carriers with and without FXTAS. In the FXTAS group, all 4 subcortical structures under investigation (ie, the thalamus, caudate nucleus, putamen, and globus pallidus) exhibited volume atrophy compared with the control group. Some structures showed potential iron deposition, manifested as DWI signal reduction. The FXTAS group also displayed significant volume reduction and DWI signal loss in the thalamus and striatum compared with the non-FXTAS premutation group. In comparison, no differences in FA or MD were detected between the groups.

Group-mean comparisons revealed volume atrophy in all 4 structures for the FXTAS group (Table 2). This is in contrast to our previous voxel-based morphological analysis, in which only the thalamus, but not the basal ganglia, showed decreased T1-signal intensity in FXTAS carriers.[41] Improved image quality because of higher MRI static field strength (3 versus 1.5 T) and the utilization of an image-processing tool specifically designed for registering and segmenting subcortical gray matter might have contributed to the greater sensitivity in detecting the basal ganglia changes in the current investigation.

The involvement of the thalamus and basal ganglia in FXTAS is consistent with the functions carried by these structures, which extend beyond simple motor control to cognitive, motivational, and emotional processing during learning and execution of complex behaviors.[42] The basal ganglia and thalamus are the

TABLE 3. Correlation with FXTAS stage using TCV (for volume only) and age as covariates (n = 47, df = 1).

Structures	Side	Volume (100-voxel reduction)				FA (0.01-unit elevation)				DWI (1-unit reduction)			
		Odds ratio	95% CI bounds		P	Odds ratio	95% CI bounds		P	Odds ratio	95% CI bounds		P
			Lower	Upper			Lower	Upper			Lower	Upper	
Thalamus	Left	1.21	1.11	1.33	**<.001**	1.10	0.94	1.30	.30	1.05	0.99	1.11	.08
	Right	1.16	1.07	1.26	**<.001**[a]	0.97	0.83	1.14	.71	1.07	1.01	1.12	.018
Caudate	Left	1.22	1.03	1.45	**.015**	1.15	1.06	1.25	**.001**	1.05	1.01	1.10	.013[a]
	Right	1.16	1.01	1.33	.04	1.12	1.04	1.21	**.002**	1.05	1.01	1.09	.021
Putamen	Left	1.27	1.14	1.41	**<.001**	1.06	0.97	1.15	.20	1.05	1.00	1.10	.06
	Right	1.21	1.09	1.35	**<.001**	1.09	0.98	1.22	.14	1.08	1.02	**1.13**	**.003**
Pallidus	Left	1.19	0.94	1.51	.12	0.99	0.93	1.05	.71	1.03	0.98	1.09	.28
	Right	1.23	1.01	1.50	.03	1.02	0.96	1.08	.62	1.02	0.97	1.07	.38

In boldface, significant at 5% FDR, $P \leq .017$.
[a]Fail to pass likelihood ratio test at α = 0.05 for testing the same slope coefficients across different levels of FXTAS stage. For a 100-voxel reduction in volume, the odds ratio of 1.21 corresponds to a 21% increase in odds of being in higher categories of FXTAS stage.

central components of the cortical-basal ganglia-thalamic-cortical network.[42,43] Although all areas of the neocortex provide input to the basal ganglia, which in turn projects massively to the thalamus, thalamic output mostly targets the frontal cortex, with the temporal, parietal, and brain stem areas receiving minor output. This asymmetric information flow suggests a general-purpose role of the basal ganglia and thalamus in performing information sorting, integration, and redirection for high-level processing in the frontal cortex.[42-44] Thus, structural damage in the thalamus and basal ganglia can cause a profound effect on various types of brain processing and may contribute to functional deficits in FXTAS that include not only motor, but also cognitive, social, and emotional processing.[7-9,45]

Given the high negative correlation between DWI signal intensity and iron concentration in the thalamus and putamen,[26] we examined DWI signal intensity and found significant reduction in the thalamus and basal ganglia in the FXTAS group (Table 2). The DWI signal reduction was especially robust in the bilateral caudate, as the group differences remained significant ($t = -4.02$ and -3.88, $P = .0002$ and .0003, respectively, for left and right) after adding volume as an additional covariate to account for the effect of the same amount of iron contained in shrinking tissues. The biochemical reports of mitochondrial dysfunction in the fibroblasts and cortical neurons from premutation carriers with and without FXTAS[15,16] corroborated well with our results. Dysregulated zinc and iron metabolisms disrupt mitochondrial function. One of the downstream consequences is iron accumulation in the cells, which is supported by the improved mitochondrial function in fibroblasts treated with both zinc supplementation and an iron chelator.[16]

With regard to the association with FXTAS stage, we found that more advanced stages of FXTAS were associated with volume atrophy in the thalamus and striatum and DWI signal reduction in the putamen, indicating gradual tissue loss and iron accumulation as motor function becomes more impaired (Table 3). In addition, the bilateral caudate nucleus showed significant positive correlation between FA and FXTAS stage, an apparently counterintuitive finding. We performed further correlational analysis and found negative correlations between caudate FA and volume ($r = -0.55$, $P < .001$), MD ($r = -0.49$, $P < .001$), and DWI ($r = -0.29$, $P = .051$). The head of the caudate, contributing the most to the caudate measurements, contains the frontal-striatal pathway. The patterns of change may indicate preferential loss of striatal cell bodies and a relatively spared frontal-striatal pathway in FXTAS. Longitudinal studies tracking patients from early to advanced stages of FXTAS are necessary to confirm this interpretation.

As we were using MRI scans acquired from 2007 to 2009, the most significant limitation of the current study was not being able to use an MRI sequence designed specifically for quantifying iron deposition. Consequently, the results regarding iron accumulation need to be confirmed using a standard imaging technique, for instance, the susceptibility-weighted imaging, $R2^*$, and field-dependent relaxation increase (FDRI).[19,46-49] In addition, intermodal image registration is challenging, especially in the case of EPI sequences with substantial susceptibility-related distortion. Although considerable effort and care were taken to manually adjust the registration, minor errors may still exist. Other limitations include the inability of DTI to pinpoint the exact type of damage that has occurred in tissues containing a mixture of cell bodies and axons. As we analyzed the thalamus as a whole, our findings may not be applicable to all thalamic nuclei, each of which connects with distinct cortical and subcortical structures to support diverse brain functions. We are currently conducting DTI tractography-based segmentation of the thalamus[50] to further identify the nuclei that are especially vulnerable to FXTAS.

In conclusion, this study revealed critical involvement of the thalamus and basal ganglia in FXTAS. All 4 structures exhibited changes in a multitude of measurements in the FXTAS group. Importantly, thalamic and striatal measurements demonstrated functional significance by showing significant correlation with FXTAS stage. These results indicate the need for further studies to verify the benefit of tracking structural changes in subcortical gray matter for making prognosis, monitoring disease progression, and determining the effectiveness of therapeutic treatment of FXTAS.

References

1. Verkerk AJ, Pieretti M, Sutcliffe JS, et al. Identification of a gene (FMR-1) containing a CGG repeat coincident with a breakpoint cluster region exhibiting length variation in fragile X syndrome. Cell. 1991;65:905–914.

2. Dombrowski C, Levesque S, Morel ML, Rouillard P, Morgan K, Rousseau F. Premutation and intermediate-size FMR1 alleles in 10572 males from the general population: loss of an AGG interruption is a late event in the generation of fragile X syndrome alleles. Hum Mol Genet. 2002;11:371–378.

3. Toledano-Alhadef H, Basel-Vanagaite L, Magal N, et al. Fragile-X carrier screening and the prevalence of premutation and full-mutation carriers in Israel. Am J Hum Genet. 2001;69:351–360.

4. Fernandez-Carvajal I, Walichiewicz P, Xiaosen X, Pan R, Hagerman PJ, Tassone F. Screening for expanded alleles of the FMR1 gene in blood spots from newborn males in a Spanish population. J Mol Diagn. 2009;11:324–329.

5. Hagerman RJ, Leehey M, Heinrichs W, et al. Intention tremor, parkinsonism, and generalized brain atrophy in male carriers of fragile X. Neurology. 2001;57:127–130.

6. Jacquemont S, Hagerman RJ, Leehey MA, et al. Penetrance of the fragile X-associated tremor/ataxia syndrome in a premutation carrier population. JAMA. 2004;291:460–469.

7. Bourgeois JA, Seritan AL, Casillas EM, et al. Lifetime prevalence of mood and anxiety disorders in fragile X premutation carriers. J Clin Psychiatry. 2010;72:175–182.

8. Brega AG, Goodrich G, Bennett RE, et al. The primary cognitive deficit among males with fragile X-associated tremor/ataxia syndrome (FXTAS) is a dysexecutive syndrome. J Clin Exp Neuropsychol. 2008;30:853–869.

9. Jacquemont S, Hagerman RJ, Leehey M, et al. Fragile X premutation tremor/ataxia syndrome: molecular, clinical, and neuroimaging correlates. Am J Hum Genet. 2003;72:869–878.

10. Juncos JL, Lazarus JT, Graves-Allen E, et al. New clinical findings in the fragile X-associated tremor ataxia syndrome (FXTAS). Neurogenetics. 2011;12:123–135.

11. Soontarapornchai K, Maselli R, Fenton-Farrell G, et al. Abnormal nerve conduction features in fragile X premutation carriers. Arch Neurol. 2008;65:495–498.

12. Greco CM, Berman RF, Martin RM, et al. Neuropathology of fragile X-associated tremor/ataxia syndrome (FXTAS). Brain. 2006;129:243–255.

13. Greco CM, Hagerman RJ, Tassone F, et al. Neuronal intranuclear inclusions in a new cerebellar tremor/ataxia syndrome among fragile X carriers. Brain. 2002;125:1760–1771.

14. Hunsaker MR, Greco CM, Spath MA, et al. Widespread non-central nervous system organ pathology in fragile X premutation carriers with fragile X-associated tremor/ataxia syndrome and CGG knock-in mice. Acta Neuropathol. 2011;122:467–479.

15. Ross-Inta C, Omanska-Klusek A, Wong S, et al. Evidence of mitochondrial dysfunction in fragile X-associated tremor/ataxia syndrome. Biochem J. 2010;429:545–552.

16. Napoli E, Ross-Inta C, Wong S, et al. Altered zinc transport disrupts mitochondrial protein processing/import in fragile X-associated tremor/ataxia syndrome. Hum Mol Genet. 2011;20:3079–3092.

17. Loesch DZ, Godler DE, Evans A, et al. Evidence for the toxicity of bidirectional transcripts and mitochondrial dysfunction in blood associated with small CGG expansions in the FMR1 gene in patients with parkinsonism. Genet Med. 2011;13:392–399.

18. Dusek P, Jankovic J, Le W. Iron dysregulation in movement disorders. Neurobiol Dis. 2012;46:1–18.

19. Haacke EM, Cheng NY, House MJ, et al. Imaging iron stores in the brain using magnetic resonance imaging. Magn Reson Imaging. 2005;23:1–25.

20. Hallgren B, Sourander P. The effect of age on the non-haemin iron in the human brain. J Neurochem. 1958;3:41–51.

21. Pujol J, Junque C, Vendrell P, et al. Biological significance of iron-related magnetic resonance imaging changes in the brain. Arch Neurol. 1992;49:711–717.

22. Hashimoto R, Srivastava S, Tassone F, Hagerman RJ, Rivera SM. Diffusion tensor imaging in male premutation carriers of the fragile X mental retardation gene. Mov Disord. 2011;26:1329–1336.

23. Wang JY, Hessl DH, Hagerman RJ, Tassone F, Rivera SM. Age-dependent structural connectivity effects in fragile x premutation. Arch Neurol. 2012;69:482–489.

24. Basser PJ, Mattiello J, LeBihan D. Estimation of the effective self-diffusion tensor from the NMR spin echo. J Magn Reson B. 1994;103:247–254.

25. Basser PJ, Pierpaoli C. Microstructural and physiological features of tissues elucidated by quantitative-diffusion-tensor MRI. J Magn Reson B. 1996;111:209–219.

26. Pfefferbaum A, Adalsteinsson E, Rohlfing T, Sullivan EV. Diffusion tensor imaging of deep gray matter brain structures: effects of age and iron concentration. Neurobiol Aging. 2010;31:482–493.

27. Du G, Lewis MM, Styner M, et al. Combined $R2^*$ and diffusion tensor imaging changes in the substantia nigra in Parkinson's disease. Mov Disord. 2011;26:1627–1632.

28. Behrens TE, Johansen-Berg H, Woolrich MW, et al. Non-invasive mapping of connections between human thalamus and cortex using diffusion imaging. Nat Neurosci. 2003;6:750–757.

29. Lehericy S, Ducros M, Van de Moortele PF, et al. Diffusion tensor fiber tracking shows distinct corticostriatal circuits in humans. Ann Neurol. 2004;55:522–529.

30. Connor JR, Menzies SL, Burdo JR, Boyer PJ. Iron and iron management proteins in neurobiology. Pediatr Neurol. 2001;25:118–129.

31. Moseley ME, Kucharczyk J, Mintorovitch J, et al. Diffusion-weighted MR imaging of acute stroke: correlation with T2-weighted and magnetic susceptibility-enhanced MR imaging in cats. AJNR Am J Neuroradiol. 1990;11:423–429.

32. Ebisu T, Naruse S, Horikawa Y, et al. Discrimination between different types of white matter edema with diffusion-weighted MR imaging. J Magn Reson Imaging. 1993;3:863–868.

33. Filipovic-Sadic S, Sah S, Chen L, et al. A novel FMR1 PCR method for the routine detection of low abundance expanded alleles and full mutations in fragile X syndrome. Clin Chem. 2010;56:399–408.

34. Tassone F, Hagerman RJ, Taylor AK, Gane LW, Godfrey TE, Hagerman PJ. Elevated levels of FMR1 mRNA in carrier males: a new mechanism of involvement in the fragile-X syndrome. Am J Hum Genet. 2000;66:6–15.

35. Tassone F, Hagerman R. The fragile X-associated tremor ataxia syndrome. Results Probl Cell Differ. 2012;54:337–357.

36. Patenaude B, Smith SM, Kennedy DN, Jenkinson M. A Bayesian model of shape and appearance for subcortical brain segmentation. Neuroimage. 2011;56:907–922.

37. Smith SM, Jenkinson M, Woolrich MW, et al. Advances in functional and structural MR image analysis and implementation as FSL. Neuroimage. 2004;23(Suppl 1):S208–S219.

38. Smith SM, Zhang Y, Jenkinson M, et al. Accurate, robust, and automated longitudinal and cross-sectional brain change analysis. Neuroimage. 2002;17:479–489.

39. Benjamini Y, Hochberg Y. Controlling the false discovery rate—a practical and powerful approach to multiple testing. J R Stat Soc Series B Stat Methodol. 1995;57:289–300.

40. O'Brien RG. A simple test for variance effects in experimental designs. Psychol Bull. 1981;89:570–574.

41. Hashimoto R, Javan AK, Tassone F, Hagerman RJ, Rivera SM. A voxel-based morphometry study of grey matter loss in fragile X-associated tremor/ataxia syndrome. Brain. 2011;134:863–878.

42. Haber SN, Calzavara R. The cortico-basal ganglia integrative network: the role of the thalamus. Brain Res Bull. 2009;78:69–74.

43. Graybiel AM. The basal ganglia. Curr Biol. 2000;10:R509–R511.

44. Stocco A, Lebiere C, Anderson JR. Conditional routing of information to the cortex: a model of the basal ganglia's role in cognitive coordination. Psychol Rev. 2010;117:541–574.

45. Cornish K, Kogan C, Turk J, et al. The emerging fragile X premutation phenotype: evidence from the domain of social cognition. Brain Cogn. 2005;57:53–60.

46. Bartzokis G, Aravagiri M, Oldendorf WH, Mintz J, Marder SR. Field dependent transverse relaxation rate increase may be a specific measure of tissue iron stores. Magn Reson Med. 1993;29:459–464.

47. Bilgic B, Pfefferbaum A, Rohlfing T, Sullivan EV, Adalsteinsson E. MRI estimates of brain iron concentration in normal aging using quantitative susceptibility mapping. Neuroimage. 2012;59:2625–2635.

48. Haacke EM, Xu Y, Cheng YC, Reichenbach JR. Susceptibility weighted imaging (SWI). Magn Reson Med. 2004;52:612–618.

49. Langkammer C, Krebs N, Goessler W, et al. Quantitative MR imaging of brain iron: a postmortem validation study. Radiology. 2010;257:455–462.

50. Johansen-Berg H, Behrens TE, Sillery E, et al. Functional-anatomical validation and individual variation of diffusion tractography-based segmentation of the human thalamus. Cereb Cortex. 2005;15:31–39.